iScience

CellPress

Article

Chemogenetic Activation of Prefrontal Cortex in *Shank3*-Deficient Mice Ameliorates Social Deficits, NMDAR Hypofunction, and Sgk2 Downregulation

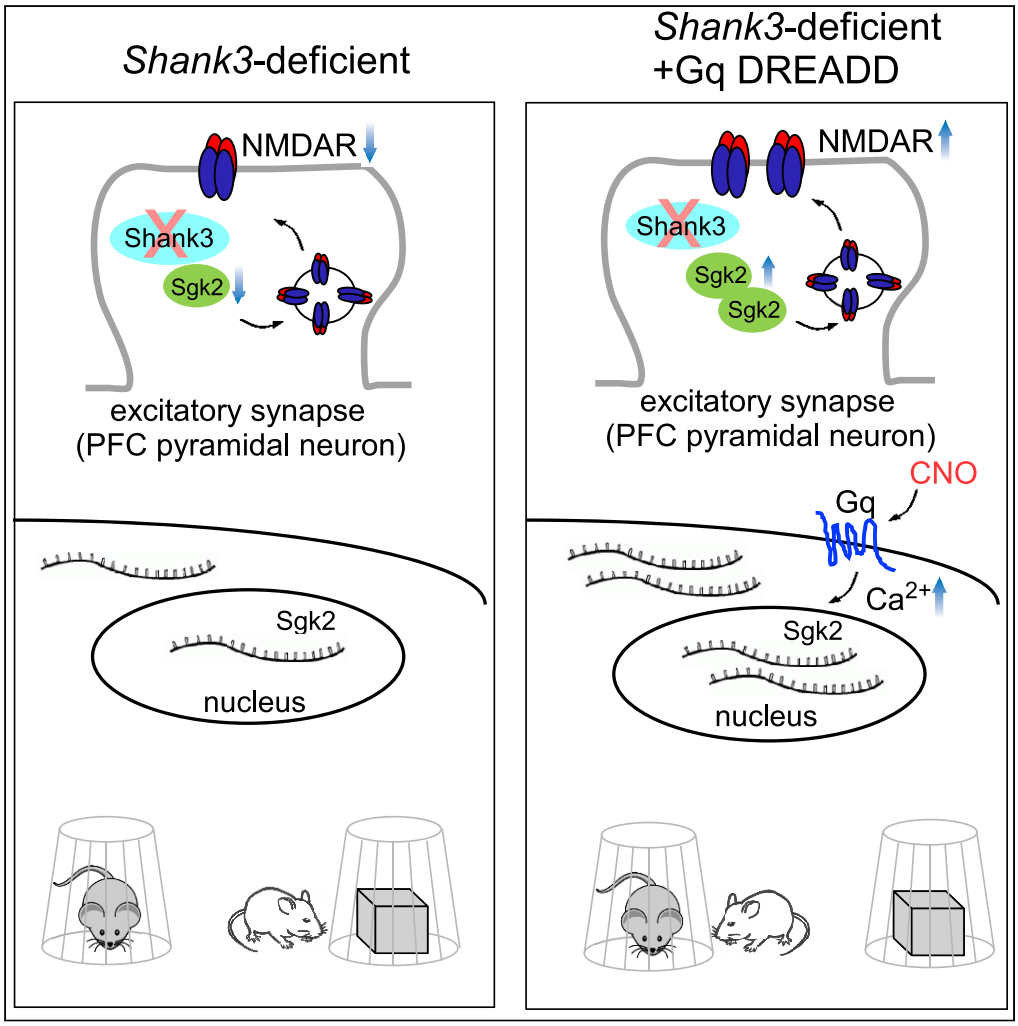

Luye Qin, Kaijie Ma, Zhen Yan

zhenyan@buffalo.edu

HIGHLIGHTS

Chemogenetic activation of PFC rescues social deficits in *Shank3*-deficient mice

Gq DREADD restores NMDAR and elevates AMPAR signaling in PFC of *Shank3*-deficient mice

Gq DREADD recovers serum- and glucocorticoid-inducible kinase 2 (Sgk2) expression

Sgk is required for chemogenetic rescue of social deficits and NMDAR hypofunction

Qin et al., iScience *17*, 24–35
July 26, 2019
https://doi.org/10.1016/j.isci.2019.06.014

iScience

CellPress

Article

Chemogenetic Activation of Prefrontal Cortex in *Shank3*-Deficient Mice Ameliorates Social Deficits, NMDAR Hypofunction, and Sgk2 Downregulation

Luye Qin,[1] Kaijie Ma,[1] and Zhen Yan[1,2,*]

SUMMARY

Haploinsufficiency of the *SHANK3* gene is causally linked to autism spectrum disorders (ASDs) in human genetic studies. Here we found that chemogenetic activation of pyramidal neurons in the prefrontal cortex (PFC) of *Shank3*-deficient mice with the hM3D (Gq) DREADD restored social preference behaviors and elevated glutamatergic synaptic function in PFC. Moreover, the expression of Sgk2 (serum- and glucocorticoid-inducible kinase 2), a member of the Sgk family, which plays a key role in regulating the membrane trafficking of glutamate receptors, was diminished by Shank3 deficiency and rescued by Gq DREADD activation of PFC. Blocking Sgk function in *Shank3*-deficient mice prevented Gq DREADD from rescuing social and synaptic deficits, whereas blocking Sgk function in wild-type mice led to the attenuation of PFC glutamatergic signaling and the induction of autism-like social deficits. These results have provided a potential circuit intervention and molecular target for autism treatment.

INTRODUCTION

Autism spectrum disorders (ASDs) are a group of neurodevelopmental disorders characterized by persistent deficits in social communication and interaction, as well as restricted, repetitive patterns of behavior, interests, or activities. At present, there is no US Food and Drug Administration-approved medical treatment for core symptoms of ASDs, which makes the discovery of novel interventions an important undertaking in ASD research (Lee et al., 2016).

One of the key brain regions impaired in ASDs is the prefrontal cortex (PFC), which mediates "high-level" executive functions, including working memory, sustained attention, decision making, and emotional control (Davidson, 2002; Arnsten and Rubia, 2012). Glutamatergic transmission is pivotal for PFC-dependent functions, and disturbed glutamatergic system in frontal cortex has been identified in patients with ASD (Stoner et al., 2014). One of ASD risk factors is the *N*-methyl-D-aspartate (NMDA)-type glutamate receptor (Hu et al., 2016; Rossi et al., 2017), which is required for neuronal survival, synaptic plasticity, and memory formation (Ikonomidou et al., 1999). NMDA receptor (NMDAR) blockade or NR1 deficiency induces ASD-like social deficits in mice (Zou et al., 2008; Billingslea et al., 2014; Wesseling et al., 2014).

Heterogeneous genetic variations are associated with ASD (Abrahams et al., 2013), whereas haploinsufficiency of the *Shank3* gene has been identified as a prevalent and highly penetrant monogenic cause of autism (Durand et al., 2007; Betancur and Buxbaum, 2013). *Shank3* encodes a scaffolding protein at postsynaptic density of glutamatergic synapses (Naisbitt et al., 1999; Hayashi et al., 2009). *Shank3*-deficient mouse models exhibit ASD-like phenotypes (Wang et al., 2011, 2016; Kouser et al., 2013; Duffney et al., 2015; Qin et al., 2018), as well as the significantly diminished NMDAR synaptic function in PFC (Duffney et al., 2015; Qin et al., 2018; Wang et al., 2019).

To identify the neuronal circuits and molecular targets that could be involved in ASD treatment, we used the chemogenetic tool, designer receptors exclusively activated by designer drugs (DREADDs), to manipulate the activity of PFC neurons in wild-type or *Shank3*-deficient mice. The Gq-coupled hM3Dq DREADD or Gi-coupled hM4Di DREADD, which is activated by exogenous administration of the small molecule clozapine-N-oxide (CNO), induces neuronal burst firing or neuronal silencing, respectively (Rogan and Roth, 2011). These reverse-engineered G protein-coupled receptors allow

[1]Department of Physiology and Biophysics, State University of New York at Buffalo, School of Medicine and Biomedical Sciences, Buffalo, NY 14214, USA

[2]Lead Contact

*Correspondence: zhenyan@buffalo.edu

https://doi.org/10.1016/j.isci.2019.06.014

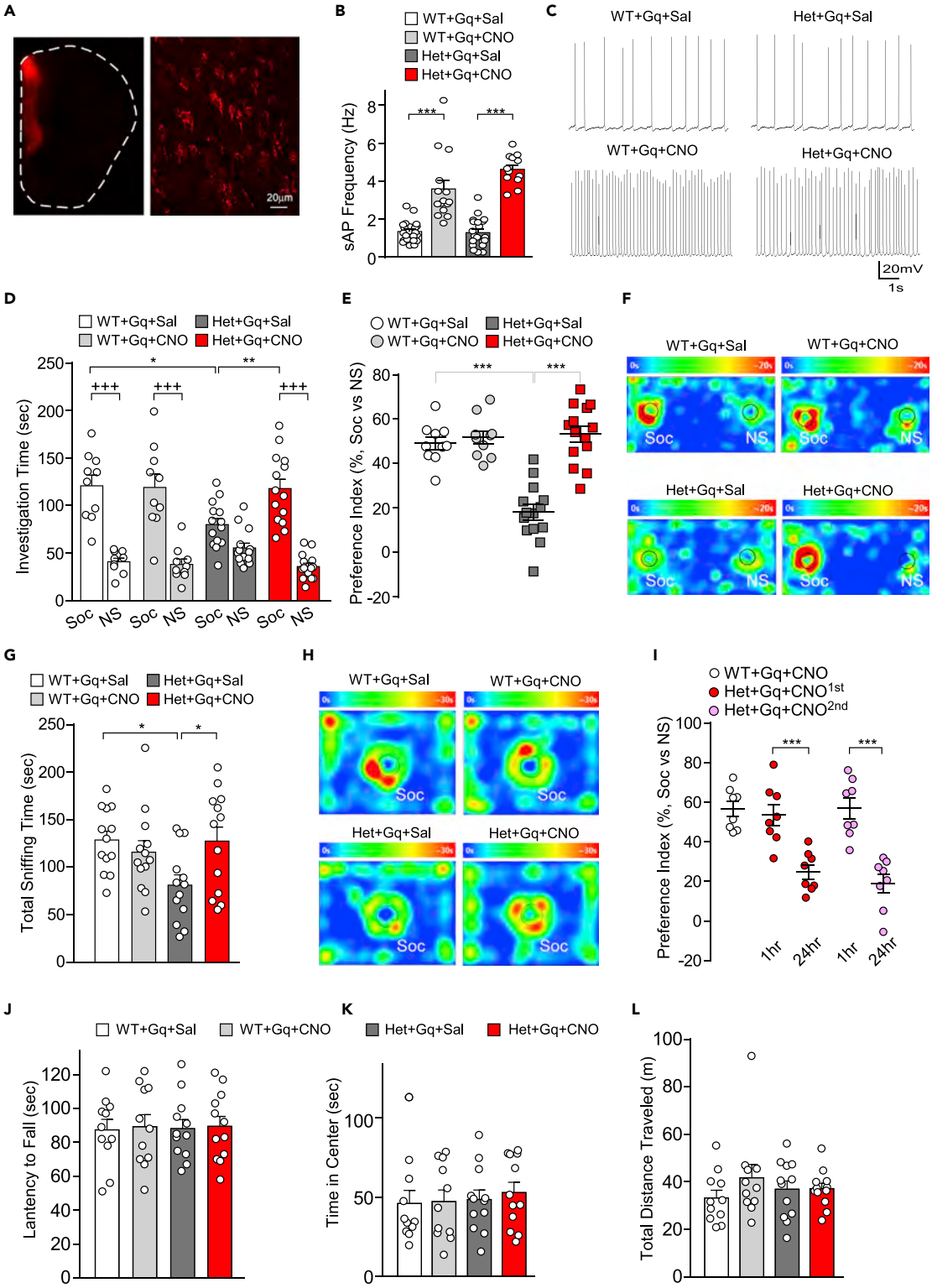

Figure 1. Chemogenetic Activation of Pyramidal Neurons in PFC Ameliorates Social Behavioral Deficits in *Shank3*-Deficient Mice

(A) Low- and high-magnification images showing hM3Dq AAV expression in PFC pyramidal neurons.

(B) Quantification of sAP frequencies in PFC pyramidal neurons from WT versus Shank3$^{+/\Delta C}$ mice (hM3Dq-injected) treated with saline or CNO (3 mg/kg, i.p.).

***$p < 0.001$, two-way ANOVA.

Figure 1. *Continued*

(C) Representative sAP traces.

(D) Bar graphs showing the time spent investigating either the social (Soc) or non-social (NS) stimulus in three-chamber sociability tests of young (5–6 weeks old) WT versus Shank3$^{+/\Delta C}$ (hM3Dq-injected) mice treated with saline or CNO. $^{+++}p < 0.001$, Soc versus NS; $^{*}p < 0.05$, $^{**}p < 0.01$, two-way ANOVA.

(E) Scatterplots showing the social preference index of the four groups. $^{***}p < 0.001$, two-way ANOVA.

(F) Representative heatmaps illustrating the time spent in different locations of the three chambers from the social preference tests.

(G) Bar graphs showing total sniffing time in social approach tests of the four groups. $^{*}p < 0.05$, two-way ANOVA.

(H) Representative heatmaps illustrating the time spent in different locations of the apparatus from the social approach tests.

(I) Scatterplots of social preference index in Shank3$^{+/\Delta C}$ mice (hM3Dq-injected) treated with CNO (two rounds) at different time points (1 h or 24 h after CNO). $^{***}p < 0.001$, ANOVA.

(J–L) Bar graphs showing a variety of behavioral tests of the four groups, including the latency to fall in rotarod tests (J), the time spent in the center in open-field tests (K), and the distance traveled in locomotion tests (L).

the remote, non-invasive, and long-lasting modulation of signal transduction pathways in discrete neuronal populations *in vivo* with therapeutic utility (Wess et al., 2013; Urban and Roth, 2015).

RESULTS

Chemogenetic Activation of PFC Pyramidal Neurons Rescues Social Behavioral Deficits in *Shank3*-Deficient Mice

Shank3-deficient mice exhibited autism-like social preference deficits (Duffney et al., 2015; Qin et al., 2018). To determine whether this behavioral abnormality can be ameliorated by activating PFC pyramidal neurons, we injected the mCherry-tagged CaMKII-driven hM3D (Gq)-coupled DREADD adeno-associated virus (AAV) (Wei et al., 2016; Wang et al., 2018) bilaterally into the medial PFC (Figure 1A). Layer 5 pyramidal neurons, which showed the clearest deficits in autistic children (Stoner et al., 2014), were selected for electrophysiological recordings (Yuen et al., 2012; Zhong and Yan, 2016; Qin et al., 2018). As shown in Figures 1B and 1C, application of CNO (3 mg/kg, intraperitoneally [i.p.]) significantly increased the frequency of spontaneous action potentials (sAPs) in hM3D(Gq)-expressing PFC pyramidal neurons in both wild-type (WT) and *Shank3*-deficient mice (WT + Gq + saline: 1.34 ± 0.12 Hz, n = 22 cells/5 mice; WT + Gq + CNO: 3.59 ± 0.46 Hz, n = 15 cells/4 mice; Shank3$^{+/\Delta C}$ + Gq + saline: 1.29 ± 0.17 Hz, n = 20 cells/5 mice; Shank3$^{+/\Delta C}$ + Gq + CNO: 4.62 ± 0.23 Hz, n = 12 cells/4 mice; $F_{1,65(\text{treatment})} = 118.7$, $p < 0.0001$, two-way ANOVA), confirming the elevation of neuronal activity by this chemogenetic approach.

Next, we examined the impact of chemogenetic activation of PFC pyramidal neurons on autism-like social deficits in young (5–6 weeks old) male Shank3$^{+/\Delta}$ mice. As shown in Figure 1D, in the three-chamber sociability assay, CNO (3 mg/kg, i.p.)-treated Shank3$^{+/\Delta}$ mice (hM3Dq-injected) spent significantly more time exploring the social stimulus over the non-social object, whereas saline-treated Shank3$^{+/\Delta C}$ mice showed a significant loss of the preference for the social stimulus and WT mice (hM3Dq-injected) treated with CNO had unchanged social preference ($F_{3,88\ (\text{interaction})} = 7.12$, $p < 0.001$, n = 10–14 each group, two-way ANOVA). Social preference index was significantly elevated in Shank3$^{+/\Delta C}$ mice after CNO treatment (Figures 1E and 1F, WT + Gq + saline: 49.1% ± 2.82%, n = 10 mice; WT + Gq + CNO: 51.7% ± 2.94%, n = 10 mice; Shank3$^{+/\Delta C}$ + Gq + saline: 18.0% ± 3.43%, n = 14 mice; Shank3$^{+/\Delta C}$ + Gq + CNO: 53.2% ± 3.50%, n = 14 mice, $F_{1,44(\text{treatment})} = 31.37$, $p < 0.001$, two-way ANOVA), indicating the dramatic alleviation of autism-like social preference deficits. To determine the specificity of the increased social preference by chemogenetic activation of PFC pyramidal neurons, we compared the preference of animals during phase I in the three-chamber sociability assay when they were exposed to two identical non-social stimuli (Duffney et al., 2015). CNO or saline-treated Shank3$^{+/\Delta C}$ mice (hM3Dq-injected) showed almost no preference on these non-social objects (preference index, Shank3$^{+/\Delta C}$ + Gq + saline: 4.4% ± 5.6%, n = 7 mice; Shank3$^{+/\Delta C}$ + Gq + CNO: 5.6% ± 4.0%, n = 9 mice, p = 0.86, t test), indicating that the increase in preference seen in Shank3$^{+/\Delta C}$ mice after DREADD excitation of the medial prefrontal cortex (mPFC) is specific for social stimuli. Although systemically injected CNO can convert to clozapine (Gomez et al., 2017), clozapine treatment (5 mg/kg, once daily for 3 days) itself failed to increase social interaction time or social preference in Shank3$^{+/\Delta}$ mice (Qin et al., 2018).

We further examined social approach behaviors in Shank3$^{+/\Delta C}$ mice with mPFC injection of hM3Dq. As shown in Figures 1G and 1H, Shank3$^{+/\Delta C}$ mice treated with CNO spent significantly more time approaching and interacting with social stimuli than saline-treated Shank3$^{+/\Delta C}$ mice, whereas CNO did not change social approach behaviors in WT mice (WT + Gq + saline: 128.8 ± 9.3 s; WT + Gq + CNO: 116 ± 12.1 s;

Shank3$^{+/\Delta C}$ + Gq + saline: 81.3 ± 10.8 s; Shank3$^{+/\Delta C}$ + Gq + CNO: 127.7 ± 14.7 s, n = 13 each group, $F_{1,48(interaction)} = 6.22$, $p < 0.05$, two-way ANOVA).

To find out the duration of the rescuing effect of chemogenetic activation of PFC pyramidal neurons, we performed social preference assays in Shank3$^{+/\Delta C}$ mice (hM3Dq-injected) at various time points after CNO treatment. The significantly increased social preference index in Shank3$^{+/\Delta C}$ mice was observed at 1 h, but not 24 h, after CNO injection, and re-injection of CNO significantly increased social preference index again, but the effect disappeared after 24 h (Figure 1I, WT + Gq + CNO: 56.7% ± 3.7%; Shank3$^{+/\Delta C}$ + Gq + first CNO: 51.2% ± 5.3% [1 h], 23.4% ± 3.5% [24 h]; Shank3$^{+/\Delta C}$ + Gq + second CNO: 56.7% ± 5.1% [1 h], 23.0% ± 4.6% [24 h]; n = 8 each group. $F_{4,35} = 17.2$, $p < 0.0001$, one-way ANOVA). These results suggest that chemogenetic activation of PFC pyramidal neurons is capable of rescuing social deficits in Shank3$^{+/\Delta C}$ mice in a fast, short-lived, but repeatable manner.

A variety of other behaviors were also examined in Shank3$^{+/\Delta C}$ mice with chemogenetic activation of PFC pyramidal neurons. As shown in Figures 1J–1L, no differences were observed in locomotion, rotarod, and open-field tests between WT and Shank3$^{+/\Delta C}$ mice (hM3Dq-injected) treated with saline or CNO (n = 11–12 each group), suggesting that CNO does not alter motor coordination or anxiety-like behaviors.

Chemogenetic Activation of PFC Pyramidal Neurons Restores NMDAR Function and Facilitates AMPAR Functions in *Shank3*-Deficient Mice

Our previous studies found that NMDAR function in PFC was selectively diminished in *Shank3*-deficient mice (Duffney et al., 2015; Qin et al., 2018). Next, we measured the impact of chemogenetic activation of PFC pyramidal neurons on NMDAR-mediated excitatory postsynaptic current (EPSC) in WT and Shank3$^{+/\Delta C}$ mice. We found that CNO treatment (1–2 h) restored the input/output curves of NMDAR-EPSC in PFC neurons of Shank3$^{+/\Delta C}$ mice (hM3Dq-injected) and elevated NMDAR-EPSC in PFC neurons of WT mice (hM3Dq-injected) (Figure 2A, $F_{3,44(treatment)} = 23.6$, $p < 0.0001$, n = 12 cells/3 mice for each group, two-way repeated measures ANOVA (rmANOVA)). No rescue of NMDAR-EPSC was found at 24 h after CNO injection (Figure S1A, $F_{3,44(treatment)} = 15.02$, $p < 0.0001$, n = 12 cells/3 mice for each group, two-way rmANOVA).

To directly visualize synaptic NMDARs, we performed immunostaining of NR2A, a major subunit of synaptic NMDARs. As shown in Figures 2B and 2C, CNO-treated Shank3$^{+/\Delta C}$ mice (hM3Dq-injected) had a significant increase in the expression level of NR2A puncta in PFC neurons, compared with saline-treated Shank3$^{+/\Delta C}$ mice (integrated intensity: WT + Gq + saline: 100 ± 7.5; WT + Gq + CNO: 124.6 ± 4.0; Shank3$^{+/\Delta C}$ + Gq + saline: 68.3 ± 4.2; Shank3$^{+/\Delta}$+Gq + CNO: 110 ± 4.4, $F_{1,42(treatment)} = 38.7$, $p < 0.0001$, n = 10–12 images/3 mice each group). Co-staining of NR2A and PSD-95 (a synaptic marker) confirmed the synaptic location of NR2A puncta (Figure S2A). These data indicate that the diminished synaptic expression and function of NMDARs in *Shank3*-deficient mice are normalized by chemogenetic activation of PFC pyramidal neurons.

For AMPAR-EPSC, no significant difference was found between saline-treated WT and Shank3$^{+/\Delta C}$ mice (hM3Dq-injected); however, CNO administration (1–2 h) significantly increased the amplitude of AMPAR-EPSC evoked by a series of stimulation intensities in both WT and Shank3$^{+/\Delta C}$ mice (Figure 3A, $F_{3,44(treatment)} = 42.7$, $p < 0.0001$, n = 12 cells/4 mice for each group, two-way rmANOVA). Spontaneous EPSC (sEPSC), a response resulting from spontaneously released glutamate, also had no difference in saline-treated WT and Shank3$^{+/\Delta C}$ mice (hM3Dq-injected), but CNO treatment markedly increased sEPSC amplitude and frequency in both genotypes (Figures 3B and 3C, WT + Gq + saline: 12.56 ± 0.37 pA, 0.8 ± 0.09 Hz, n = 10 cells/3 mice; WT + Gq + CNO: 17.66 ± 1.84 pA, 1.61 ± 0.29 Hz, n = 8 cells/3 mice; Shank3$^{+/\Delta C}$ + Gq + saline: 12.14 ± 0.29 pA, 0.75 ± 0.07 Hz, n = 10 cells/3 mice; Shank3$^{+/\Delta C}$ + Gq + CNO: 17.13 ± 2.03 pA, 1.60 ± 0.3 Hz, n = 8 cells/3 mice, $F_{1,32\ (treatment)} = 19.37$, $p = 0.0001$, two-way ANOVA). No effect on AMPAR-EPSC was observed at 24 h after CNO injection (Figure S1B, $F_{3,44\ (treatment)} = 0.38$, $p = 0.77$, n = 12 cells/3 mice for each group, two-way rmANOVA).

Immunostaining of GluR2 was also performed to visualize synaptic AMPARs. As shown in Figures 3D and 3E, despite the lack of difference in the expression level of GluR2 puncta in saline-treated WT and Shank3$^{+/\Delta}$C mice (hM3Dq-injected), CNO treatment caused a modest but significant increase of GluR2 expression in both WT and Shank3$^{+/\Delta C}$ mice (integrated intensity: WT + Gq + saline: 100 ± 2.8; WT + Gq + CNO: 115.5 ± 3.4; Shank3$^{+/\Delta C}$ + Gq + saline: 99.4 ± 5.5; Shank3$^{+/\Delta C}$ + Gq + CNO: 123.8 ± 2.8,

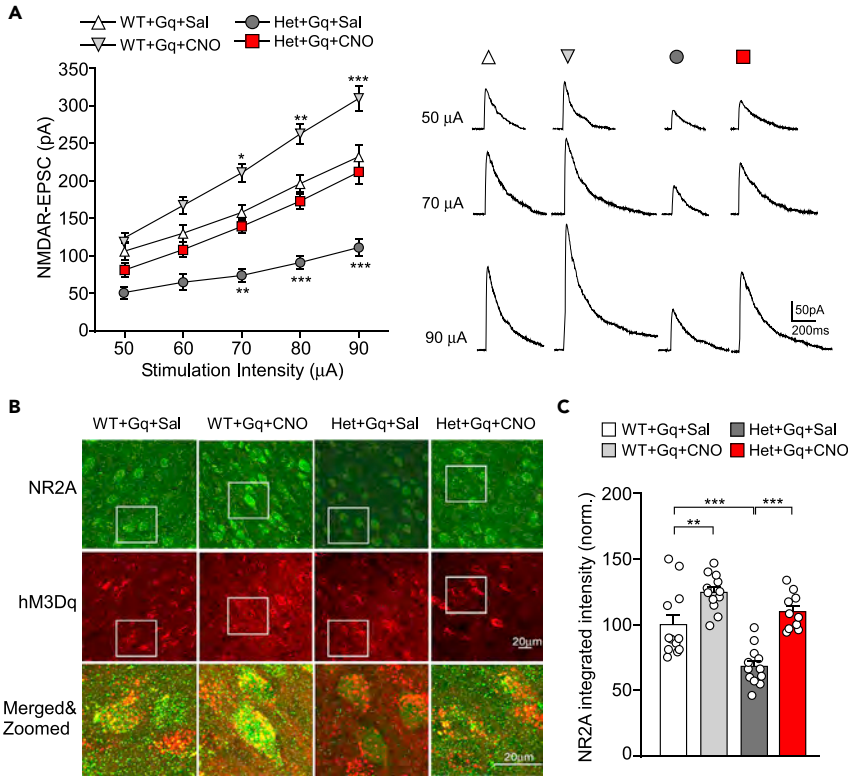

Figure 2. Chemogenetic Activation of PFC Pyramidal Neurons Restores NMDAR Function and Synaptic Expression in *Shank3*-Deficient Mice

(A) Summarized input-output curves of NMDAR-EPSC in layer V PFC pyramidal neurons from WT versus Shank3$^{+/\Delta C}$ mice (hM3Dq-injected) treated with saline or CNO. *p < 0.05, **p < 0.01, ***p < 0.001, two-way rmANOVA.

(B) Confocal images (40×) of NR2A staining in PFC slices from the four groups.

(C) Quantification of the integrated intensity of NR2A puncta in the four groups. ***p < 0.001, **p < 0.01, two-way ANOVA.

$F_{1,42(treatment)}$ = 29.7, p < 0.0001, n = 10–13 images/3 mice each group). The synaptic location of GluR2 puncta was confirmed by co-staining of GluR2 with PSD-95 (Figure S2B). These results indicate that the synaptic expression and function of AMPARs are elevated by chemogenetic activation of PFC pyramidal neurons.

Sgk Is Required for Chemogenetic Rescue of Social and Synaptic Deficits in *Shank3*-Deficient Mice, as well as for Normal Synaptic Function and Social Behaviors in WT Mice

Next, we examined potential molecular mechanisms underlying the rescuing effect of chemogenetic activation of PFC pyramidal neurons in *Shank3*-deficient mice. Our previous studies have found that the synaptic delivery of NMDARs is impaired in PFC neurons of Shank3$^{+/\Delta C}$ mice (Duffney et al., 2015; Qin et al., 2018), and the membrane trafficking of glutamate receptors is facilitated by serum- and glucocorticoid-inducible kinases (Sgk, Yuen et al., 2011). Sgk is a family of immediate-early genes and serine/threonine kinases, which plays an important role in the regulation of ion channels, enzyme activity, gene transcription, hormone release, and neuroexcitability (Lang et al., 2006). The onset kinetics of the CNO effect (>1 h) is consistent with the time frame of Sgk activation, suggesting the potential involvement of Sgk in the chemogenetic rescue.

We first compared the expression level of Sgk in WT and Shank3$^{+/\Delta C}$ mice (hM3Dq injected) treated with saline or CNO (1–2 h). Other related molecules, including calcium- and calmodulin-dependent protein kinase II (CaMKII), Src family tyrosine kinase Fyn, mGluR- and Shank-interacting protein Homer1, and activity-regulated cytoskeleton-associated protein Arc, were also compared. Quantitative PCR analyses (Figure 4A) showed that *Shank3* deficiency induced a significant decrease of the mRNA level of *Sgk2*, *Homer1a*,

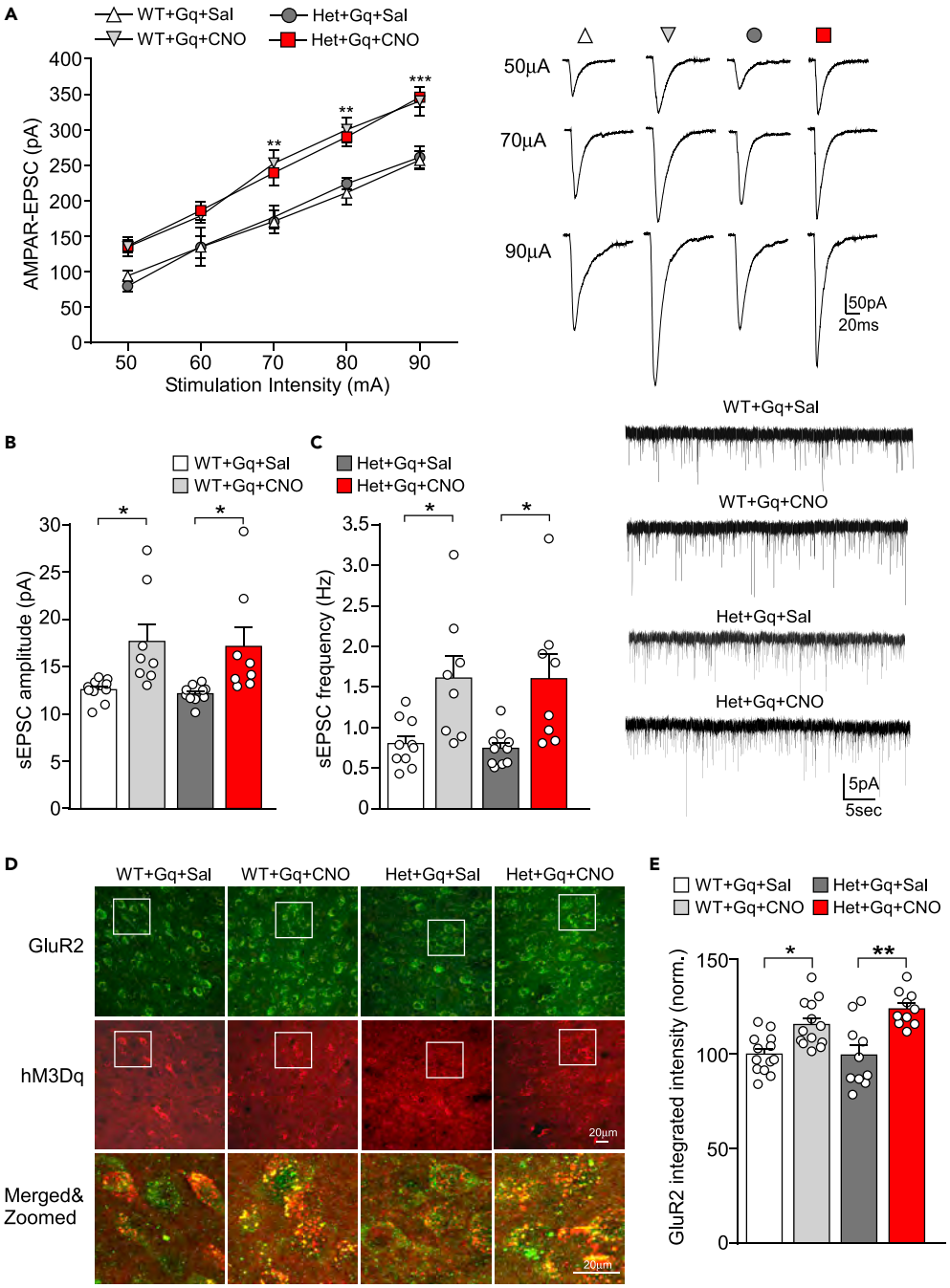

Figure 3. Chemogenetic Activation of PFC Pyramidal Neurons Facilitates AMPAR Function in *Shank3*-Deficient Mice

(A) Summarized input-output curves of AMPAR-EPSC in layer V PFC pyramidal neurons from WT versus Shank3$^{+/\Delta C}$ mice (hM3Dq-injected) treated with saline or CNO. **p < 0.01, ***p < 0.001, two-way rmANOVA.

(B and C) Bar graphs of sEPSC amplitude (B) and frequency (C) in PFC pyramidal neurons from the four groups. *p < 0.05, two-way ANOVA. Inset: representative sEPSC traces.

(D) Confocal images (40×) of GluR2 staining in PFC slices from the four groups.

(E) Quantification of the integrated intensity of GluR2 puncta in the four groups. *p < 0.05, **p < 0.01, two-way ANOVA.

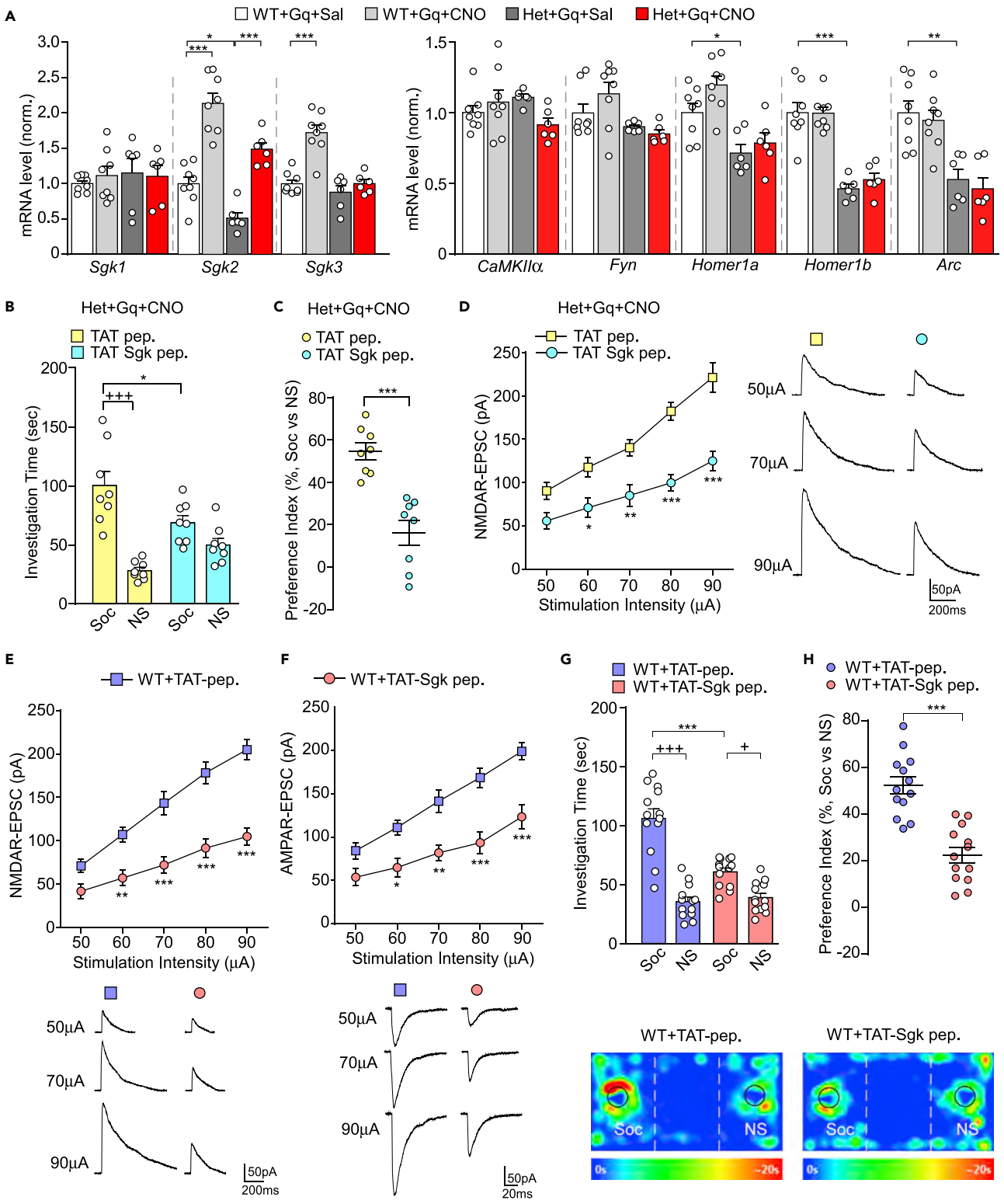

Figure 4. Sgk Is Required for Chemogenetic Rescue of Social and Synaptic Deficits in *Shank3*-Deficient Mice, as well as for Normal Synaptic Function and Social Behaviors in WT Mice

(A) Quantitative PCR data on the mRNA level of *Sgk1/2/3*, *CaMKIIα*, *Fyn*, *Homer1a/b*, and *Arc* in WT versus Shank3$^{+/\Delta C}$ mice (hM3Dq-injected) treated with saline or CNO (3 mg/kg, i.p.). *p < 0.05, **p < 0.01, ***p < 0.001.

Figure 4. *Continued*

(B) Bar graphs showing the time spent investigating social (Soc) or non-social (NS) stimulus in three-chamber sociability tests of Shank3$^{+/\Delta C}$ mice (hM3Dq-injected) injected (i.v.) with TAT-Sgk peptide (50 pmol/g, i.v.) or TAT peptide before CNO treatment. $^{+++}$p < 0.001, Soc versus NS; *p < 0.05, two-way ANOVA.

(C) Scatterplots showing the preference index of the sociability tests of the two groups. ***p < 0.001, t test.

(D) Summarized input-output curves of NMDAR-EPSC and representative traces in layer V PFC pyramidal neurons from the two groups, *p < 0.05, **p < 0.01, ***p < 0.001, two-way rmANOVA.

(E and F) Summarized input-output curves of NMDAR-EPSC (E) and AMPAR-EPSC (F) and representative traces in layer V PFC pyramidal neurons from WT mice treated with TAT-Sgk peptide or TAT peptide. *p < 0.05, **p < 0.01, ***p < 0.001, two-way rmANOVA.

(G) Graphs showing the time spent investigating either the Soc or NS stimulus in 3-chamber sociability tests of WT mice injected with TAT-Sgk peptide or TAT peptide. $^{+}$p < 0.05, $^{+++}$ p < 0.001, Soc versus NS; ***p < 0.001, two-way ANOVA.

(H) Scatterplots showing the preference index of the two groups. ***p < 0.001, t test. Inset: representative heatmaps of the 3-chamber social preference test.

Homer1b, and *Arc*, but did not change the mRNA level of *Sgk1*, *Sgk3*, *CaMKIIα*, or *Fyn*. CNO treatment of Shank3$^{+/\Delta C}$ mice restored the expression of *Sgk2* ($F_{1,24\ (genotype)}$ = 82.83, p < 0.0001, $F_{1,24\ (treatment)}$ = 23.93, p < 0.0001, n = 6–8/each group, two-way ANOVA), but not *Homer1a/b* or *Arc*. The expression of these genes might require stronger or prolonged stimulation, and additional work would be needed to clarify the specific reason for the differences in expression of these genes versus *Sgk2*. CNO treatment of WT mice elevated *Sgk2* and *Sgk3* mRNA levels. The restoration of Sgk2 expression in Shank3$^{+/\Delta C}$ mice was not observed at 24 h after CNO injection (Figure S3).

To find out whether the selective restoration of Sgk2 expression is required for the behavioral and synaptic rescue by chemogenetic activation of PFC pyramidal neurons, we inhibited Sgk function in *Shank3*-deficient mice. Sgk phosphorylates serine and threonine residues in the motif R-X-R-X-X-(S/T), so we used an Sgk substrate peptide (RPRAATF), which competitively blocks the interaction of Sgk with its endogenous substrates. The peptide was coupled to the protein transduction domain of the human immunodeficiency virus (HIV) TAT protein (YGRKKRRQRRR), which rendered it cell and blood-brain barrier permeant. Our previous studies have shown that Sgk function in PFC neurons can be inhibited by the systemic injection (intravenous [i.v.]) of the TAT-Sgk peptide (Yuen et al., 2011).

Shank3$^{+/\Delta C}$ mice (hM3Dq-injected) were injected with TAT-Sgk peptide (50 pmol/g, i.v.) or a control TAT peptide at 30 min before CNO treatment. From the three-chamber sociability assay, we found that in Shank3$^{+/\Delta C}$ mice injected with TAT-Sgk peptide, CNO (3 mg/kg, i.p.) treatment failed to elevate the social interaction time (Figure 4B, TAT-Sgk peptide: 68.9 ± 6.2 s (Soc [social]), 50 ± 5.6 s (NS [non-social]); TAT-peptide, 101 ± 12 s (Soc), 28.3 ± 2.8 s (NS), n = 8/group; $F_{1,\ 28\ (interaction)}$ = 12.8, p < 0.01, two-way ANOVA) and failed to restore the social preference index (Figure 4C, TAT-Sgk peptide: 16.2% ± 5.9%, n = 8, TAT peptide: 54.7% ± 4.0%, n = 8, p < 0.001, t test). In addition, electrophysiological studies found that CNO failed to restore NMDAR-EPSC in Shank3$^{+/\Delta C}$ mice injected with TAT-Sgk peptide, but not TAT control peptide (Figure 4D, $F_{1,22\ (treatment)}$ = 25.91, n = 12 cells/3 mice each group, p < 0.001, two-way rmANOVA). These data suggest that Sgk is required for the chemogenetic rescue of social deficits and NMDAR hypofunction in *Shank3*-deficient mice.

To further test the causal role of Sgk in synaptic and social deficits associated with autism, we inhibited Sgk function in WT mice and examined its impact on synaptic function and social behaviors. We found that TAT-Sgk peptide injection (50 pmol/g, i.v.) to WT mice caused a significant reduction of NMDAR-EPSC (Figure 4E, n = 16 cells/4 mice each group, $F_{1,30\ (treatment)}$ = 26.53, p < 0.001, two-way rmANOVA) and AMPAR-EPSC (Figure 4F, n = 12 cells/4 mice each group, $F_{1,22\ (treatment)}$ = 18.88, p < 0.001, two-way rmANOVA) in PFC pyramidal neurons. In the three-chamber sociability assay, WT mice injected with TAT-Sgk peptide exhibited significantly reduced social interaction time (Figure 4G, TAT peptide: 106 ± 8.1 s, TAT-Sgk peptide: 60.8 ± 3.4 s, n = 13 pairs; $F_{1,\ 48(interaction)}$ = 22.58, p < 0.001, two-way ANOVA) and social preference index (Figure 4H, TAT peptide: 50.1% ± 3.3%; TAT-Sgk peptide: 23.1% ± 3.0%. n = 13 pairs, p < 0.001, t test). Taken together, these results have provided evidence showing the necessity and sufficiency of Sgk in the regulation of glutamatergic synaptic functions and social behaviors.

Chemogenetic Inhibition of PFC Pyramidal Neurons in WT Mice Is Insufficient to Induce Autism-like Social Deficits and Change Sgk Expression

As chemogenetic activation of PFC with hM3D(Gq) rescued social deficits in Shank3-deficient mice, we further tested whether chemogenetic inactivation of PFC is able to induce autism-like social deficits in WT mice. The mCherry-tagged CaMKII-driven Gi-coupled hM4-muscarinic receptor (hM4Di AAV), which

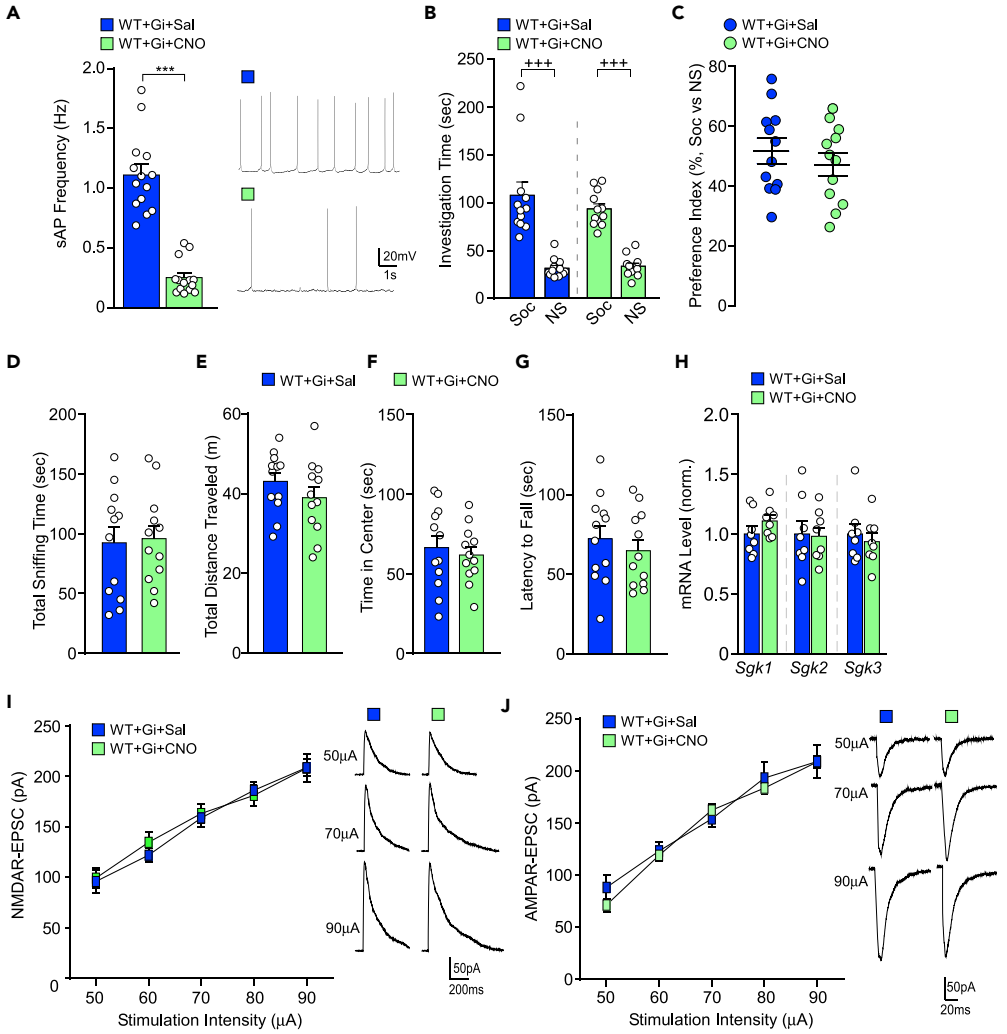

Figure 5. Chemogenetic Inhibition of PFC Pyramidal Neurons in WT Mice Fails to Induce Autism-like Social Deficits and Changes Sgk Expression

(A) Quantification of sAP frequencies in PFC pyramidal neurons from WT mice (hM4Di-injected) treated with saline or CNO (3 mg/kg, i.p.). ***$p < 0.001$, t test. Inset: representative sAP traces.

(B) Bar graphs showing the time spent investigating social (Soc) or non-social (NS) stimulus in three-chamber sociability tests of WT mice (hM4Di-injected) treated with saline or CNO. $^{+++}p < 0.001$, Soc versus NS, two-way ANOVA.

(C) Scatterplots showing the social preference index of the two groups.

(D) Bar graphs showing total sniffing time in social approach tests of the two groups.

(E–G) Bar graphs showing a variety of behaviors of the two groups, including the distance traveled in locomotion tests (E), the time spent in the center during open-field tests (F), and the latency to fall during rotarod tests (G).

(H) Quantitative PCR data on the mRNA level of Sgk1, Sgk2, and Sgk3 in PFC of the two groups.

(I and J) Summarized input-output curves of NMDAR-EPSC (I) or AMPAR-EPSC (J) in layer V PFC pyramidal neurons from WT mice (hM4Di-injected) treated with saline or CNO (3 mg/kg, i.p.).

induces neuronal silencing upon its activation by CNO (Urban and Roth, 2015), was injected bilaterally into the medial PFC of WT mice. Application of CNO (3 mg/kg, i.p.) significantly decreased the frequency of sAP in PFC pyramidal neurons of hM4Di-injected WT mice (Figure 5A, WT + Gi + saline: 1.11 ± 0.09 Hz, n = 14 cells/4 mice; WT + Gi + CNO: 0.25 ± 0.04 Hz, n = 14 cells/4 mice; $p < 0.0001$, t test), confirming the inhibitory effect of this chemogenetic approach.

In the three-chamber sociability test, WT mice (hM4Di-injected) treated with CNO (3 mg/kg, i.p) or saline had similar social interaction time (Figure 5B, n = 12 pairs) and social preference index (Figure 5C, $p > 0.05$,

t test). Social approach behavior was unchanged by CNO treatment of WT mice (Figure 5D, n = 12 pairs). Locomotion, rotarod, and open-field tests also failed to find differences between CNO and saline-injected WT mice (Figures 5E–5G, n = 12 pairs). Moreover, quantitative PCR analyses showed no significant difference in the mRNA level of Sgk1, Sgk2, and Sgk3 between WT mice (hM4Di-injected) treated with CNO and saline (Figure 5H, n = 8 pairs). Next, we examined the impact of chemogenetic inactivation of PFC pyramidal neurons on glutamatergic transmission. No significant difference was found in WT mice (hM4Di-injected) treated with CNO (1–2 h) or saline on NMDAR-EPSC (Figure 5I, $F_{1,\ 22\ (treatment)} = 0.09$, $p = 0.76$, n = 12 cells/3 mice for each group, two-way rmANOVA) or AMPAR-EPSC (Figure 5J, $F_{1,\ 22\ (treatment)} = 0.23$, $p = 0.64$, n = 12 cells/3 mice for each group, two-way rmANOVA). These results suggest that dampening the PFC neuronal activity in WT mice is not sufficient to induce autism-like social deficits, which could be due to the lack of changes in Sgk expression and NMDAR function. These results are consistent with prior optogenetic studies that inhibiting mPFC does not disrupt normal social preference in WT mice (Yizhar et al., 2011).

DISCUSSION

Using the DREADD-based strategy, which has the capability to precisely control long-range and local neural network (Alexander et al., 2009; Michaelides et al., 2013; Wess et al., 2013; Urban and Roth, 2015), we have found that chemogenetic activation of PFC pyramidal neurons rescues autism-like social deficits in *Shank3*-deficient mice. Consistently, cognitive and social impairments in another autism model, transgenic mice carrying 16p11.2 deletion (*16p11*$^{+/-}$), are also ameliorated by elevating PFC neuronal activity with Gq-coupled DREADD (Wang et al., 2018). It suggests that manipulating key neuronal circuits could be an effective avenue to alleviate behavioral abnormalities of ASD.

The behavioral effects of chemogenetic activation of PFC pyramidal neurons in *Shank3*-deficient mice are associated with the restoration or facilitation of NMDAR and AMPAR synaptic function, consistent with the implication of glutamatergic deficits in ASD (Wang et al., 2011, 2016; Kouser et al., 2013; Duffney et al., 2015; Qin et al., 2018). The membrane trafficking of glutamate receptors is regulated by a wide variety of molecules, including scaffolding proteins, synaptic plasticity genes like Arc, and protein kinases like CaMKII, Fyn, and Sgk (Prybylowski et al., 2005; Chowdhury et al., 2006; Yuen et al., 2011). Dysregulated NMDAR trafficking and synaptic efficacy are suggested to contribute to neuropsychiatric disorders like schizophrenia and stress-related diseases (Lau and Zukin, 2007; Popoli et al., 2011).

In search of potential molecular targets that are involved in Shank3 deficiency-induced loss of synaptic NMDARs and chemogenetic elevation of NMDAR and AMPAR function, we have found that only the Sgk family member Sgk2 shows diminished expression in *Shank3*-deficient mice, which is rescued by Gq-DREADD. Sgk is a family of serine/threonine kinase that plays a key role in regulating the trafficking of ion channels and transporters (Lang et al., 2006). Our previous studies have shown that stimulation of Sgk transcription elevates the expression of surface NMDARs and AMPARs (Yuen et al., 2011) by facilitating Rab4-mediated recycling of glutamate receptors to the synaptic membrane (Liu et al., 2010). Sgk is also a family of immediate-early gene that can be transcriptionally activated by stress hormones and phosphoinositide-3 kinase (PI3K) signaling pathway (Park et al., 1999). Activation of protein kinase C (PKC) has been shown to potentiate the activity of PI3K (Ziemba et al., 2016). Therefore, Gq-DREADD may elevate the mRNA level of Sgk2 via the PKC-PI3K cascade. Our discovery that blocking Sgk function in *Shank3*-deficient mice prevents Gq-DREADD from restoring NMDAR function and rescuing social deficits, and blocking Sgk function in WT mice induces the loss of PFC glutamatergic transmission and autism-like social deficits, further confirms the necessity and sufficiency of Sgk in these processes. Results gained from this study have provided insights into the circuity intervention and molecular targets for ASD treatment.

Limitation of the Study

Our evidence has suggested that the restored Sgk2 expression in *Shank3*-deficient mice induced by chemogenetic activation of PFC may contribute to the restoration or facilitation of NMDAR and AMPAR synaptic function and the rescue of social deficits; however, indirect effects cannot be ruled out. Several immediate-early genes show activity-dependent expression, and this may be responsible for the increased expression of Sgk2. Additional work would be needed to confirm that activity-dependent expression is indeed responsible for upregulation of Sgk2. The other limitation is the lack of direct visualization of the synaptic expression of NMDARs and AMPARs elevated by chemogenetic activation of PFC pyramidal neurons. Co-staining NR2A or GluR2 with PSD-95 in Gq DREADD-infected brain slices in WT or Shank3-

deficient mice would provide complementary evidence in support of the electrophysiological data, but cannot currently be performed due to technical limitations.

METHODS

All methods can be found in the accompanying Transparent Methods supplemental file.

SUPPLEMENTAL INFORMATION

Supplemental Information can be found online at https://doi.org/10.1016/j.isci.2019.06.014.

ACKNOWLEDGMENTS

This work was supported by the Nancy Lurie Marks Family Foundation and grants from the National Institutes of Health (MH112237, MH108842, and DA037618 to Z.Y.; MH116453 to L.Q.). We also thank E.F. Trachtman and the Varanasi family for their donations.

AUTHOR CONTRIBUTIONS

L.Q. performed electrophysiological, immunocytochemical, and biochemical experiments; analyzed data; and wrote the draft. K.M. performed behavioral experiments and analyzed data. Z.Y. supervised the experimental design and wrote the paper.

DECLARATION OF INTERESTS

The authors declare no competing financial interests.

Received: November 12, 2018
Revised: February 21, 2019
Accepted: June 6, 2019
Published: July 26, 2019

REFERENCES

Abrahams, B.S., Arking, D.E., Campbell, D.B., Mefford, H.C., Morrow, E.M., Weiss, L.A., Menashe, I., Wadkins, T., Banerjee-Basu, S., and Packer, A. (2013). SFARI Gene 2.0: a community-driven knowledgebase for the autism spectrum disorders (ASDs). Mol. Autism *4*, 36.

Alexander, G.M., Rogan, S.C., Abbas, A.I., Armbruster, B.N., Pei, Y., Allen, J.A., Nonneman, R.J., Hartmann, J., Moy, S.S., Nicolelis, M.A., et al. (2009). Remote control of neuronal activity in transgenic mice expressing evolved G protein-coupled receptors. Neuron *63*, 27–39.

Arnsten, A.F., and Rubia, K. (2012). Neurobiological circuits regulating attention, cognitive control, motivation, and emotion: disruptions in neurodevelopmental psychiatric disorders. J. Am. Acad. Child Adolesc. Psychiatry *51*, 356–367.

Betancur, C., and Buxbaum, J.D. (2013). SHANK3 haploinsufficiency: a "common" but underdiagnosed highly penetrant monogenic cause of autism spectrum disorders. Mol. Autism *4*, 17.

Billingslea, E.N., Tatard-Leitman, V.M., Anguiano, J., Jutzeler, C.R., Suh, J., Saunders, J.A., Morita, S., Featherstone, R.E., Ortinski, P.I., Gandal, M.J., et al. (2014). Parvalbumin cell ablation of NMDA-R1 causes increased resting network excitability with associated social and self-care deficits. Neuropsychopharmacology *39*, 1603–1613.

Chowdhury, S., Shepherd, J.D., Okuno, H., Lyford, G., Petralia, R.S., Plath, N., Kuhl, D., Huganir, R.L., and Worley, P.F. (2006). Arc/Arg3.1 interacts with the endocytic machinery to regulate AMPA receptor trafficking. Neuron *52*, 445–459.

Davidson, R.J. (2002). Anxiety and affective style: role of prefrontal cortex and amygdala. Biol. Psychiatry *51*, 68–80.

Duffney, L.J., Zhong, P., Wei, J., Matas, E., Cheng, J., Qin, L., Ma, K., Dietz, D.M., Kajiwara, Y., Buxbaum, J.D., et al. (2015). Autism-like deficits in Shank3-deficient mice are rescued by targeting actin regulators. Cell Rep. *11*, 1400–1413.

Durand, C.M., Betancur, C., Boeckers, T.M., Bockmann, J., Chaste, P., Fauchereau, F., Nygren, G., Rastam, M., Gillberg, I.C., Anckarsater, H., et al. (2007). Mutations in the gene encoding the synaptic scaffolding protein SHANK3 are associated with autism spectrum disorders. Nat. Genet. *39*, 25–27.

Gomez, J.L., Bonaventura, J., Lesniak, W., Mathews, W.B., Sysa-Shah, P., Rodriguez, L.A., Ellis, R.J., Richie, C.T., Harvey, B.K., Dannals, R.F., et al. (2017). Chemogenetics revealed: DREADD occupancy and activation via converted clozapine. Science *357*, 503–507.

Hayashi, M.K., Tang, C., Verpelli, C., Narayanan, R., Stearns, M.H., Xu, R.M., Li, H., Sala, C., and Hayashi, Y. (2009). The postsynaptic density proteins Homer and Shank form a polymeric network structure. Cell *137*, 159–171.

Hu, C., Chen, W., Myers, S.J., Yuan, H., and Traynelis, S.F. (2016). Human GRIN2B variants in neurodevelopmental disorders. J. Pharmacol. Sci. *132*, 115–121.

Ikonomidou, C., Bosch, F., Miksa, M., Bittigau, P., Vockler, J., Dikranian, K., Tenkova, T.I., Stefovska, V., Turski, L., and Olney, J.W. (1999). Blockade of NMDA receptors and apoptotic neurodegeneration in the developing brain. Science *283*, 70–74.

Kouser, M., Speed, H.E., Dewey, C.M., Reimers, J.M., Widman, A.J., Gupta, N., Liu, S., Jaramillo, T.C., Bangash, M., Xiao, B., et al. (2013). Loss of predominant Shank3 isoforms results in hippocampus-dependent impairments in behavior and synaptic transmission. J. Neurosci. *33*, 18448–18468.

Lang, F., Bohmer, C., Palmada, M., Seebohm, G., Strutz-Seebohm, N., and Vallon, V. (2006). (Patho) physiological significance of the serum- and glucocorticoid-inducible kinase isoforms. Physiol. Rev. *86*, 1151–1178.

Lau, C.G., and Zukin, R.S. (2007). NMDA receptor trafficking in synaptic plasticity and neuropsychiatric disorders. Nat. Rev. Neurosci. *8*, 413–426.

Lee, E., Lee, J., and Kim, E. (2016). Excitation/inhibition imbalance in animal models of autism spectrum disorders. Biol. Psychiatry *81*, 838–847.

Liu, W., Yuen, E.Y., and Yan, Z. (2010). The stress hormone corticosterone increases synaptic alpha-amino-3-hydroxy-5-methyl-4-isoxazolepropionic acid (AMPA) receptors via serum- and glucocorticoid-inducible kinase (SGK) regulation of the GDI-Rab4 complex. J. Biol. Chem. *285*, 6101–6108.

Michaelides, M., Anderson, S.A., Ananth, M., Smirnov, D., Thanos, P.K., Neumaier, J.F., Wang, G.J., Volkow, N.D., and Hurd, Y.L. (2013). Whole-brain circuit dissection in free-moving animals reveals cell-specific mesocorticolimbic networks. J. Clin. Invest. *123*, 5342–5350.

Naisbitt, S., Kim, E., Tu, J.C., Xiao, B., Sala, C., Valtschanoff, J., Weinberg, R.J., Worley, P.F., and Sheng, M. (1999). Shank, a novel family of postsynaptic density proteins that binds to the NMDA receptor/PSD-95/GKAP complex and cortactin. Neuron *23*, 569–582.

Park, J., Leong, M.L., Buse, P., Maiyar, A.C., Firestone, G.L., and Hemmings, B.A. (1999). Serum and glucocorticoid-inducible kinase (SGK) is a target of the PI 3-kinase-stimulated signaling pathway. EMBO J. *18*, 3024–3033.

Popoli, M., Yan, Z., McEwen, B.S., and Sanacora, G. (2011). The stressed synapse: the impact of stress and glucocorticoids on glutamate transmission. Nat. Rev. Neurosci. *13*, 22–37.

Prybylowski, K., Chang, K., Sans, N., Kan, L., Vicini, S., and Wenthold, R.J. (2005). The synaptic localization of NR2B-containing NMDA receptors is controlled by interactions with PDZ proteins and AP-2. Neuron *47*, 845–857.

Qin, L., Ma, K., Wang, Z.J., Hu, Z., Matas, E., Wei, J., and Yan, Z. (2018). Social deficits in Shank3-deficient mouse models of autism are rescued by histone deacetylase (HDAC) inhibition. Nat. Neurosci. *21*, 564–575.

Rogan, S.C., and Roth, B.L. (2011). Remote control of neuronal signaling. Pharmacol. Rev. *63*, 291–315.

Rossi, M., Chatron, N., Labalme, A., Ville, D., Carneiro, M., Edery, P., des Portes, V., Lemke, J.R., Sanlaville, D., and Lesca, G. (2017). Novel homozygous missense variant of GRIN1 in two sibs with intellectual disability and autistic features without epilepsy. Eur. J. Hum. Genet. *25*, 376–380.

Stoner, R., Chow, M.L., Boyle, M.P., Sunkin, S.M., Mouton, P.R., Roy, S., Wynshaw-Boris, A., Colamarino, S.A., Lein, E.S., and Courchesne, E. (2014). Patches of disorganization in the neocortex of children with autism. N. Engl. J. Med. *370*, 1209–1219.

Urban, D.J., and Roth, B.L. (2015). DREADDs (designer receptors exclusively activated by designer drugs): chemogenetic tools with therapeutic utility. Annu. Rev. Pharmacol. Toxicol. *55*, 399–417.

Wang, W., Rein, B., Zhang, F., Tan, T., Zhong, P., Qin, L., and Yan, Z. (2018). Chemogenetic activation of prefrontal cortex rescues synaptic and behavioral deficits in a mouse model of 16p11.2 deletion syndrome. J. Neurosci. *38*, 5939–5948.

Wang, X., McCoy, P.A., Rodriguiz, R.M., Pan, Y., Je, H.S., Roberts, A.C., Kim, C.J., Berrios, J., Colvin, J.S., Bousquet-Moore, D., et al. (2011). Synaptic dysfunction and abnormal behaviors in mice lacking major isoforms of Shank3. Mol. Genet. *20*, 3093–3108.

Wang, X., Bey, A.L., Katz, B.M., Badea, A., Kim, N., David, L.K., Duffney, L.J., Kumar, S., Mague, S.D., Hulbert, S.W., et al. (2016). Altered mGluR5-Homer scaffolds and corticostriatal connectivity in a Shank3 complete knockout model of autism. Nat. Commun. *7*, 11459.

Wang, Z.J., Zhong, P., Ma, K., Seo, J.S., Yang, F., Hu, Z., Zhang, F., Lin, L., Wang, J., Liu, T., et al. (2019). Amelioration of autism-like social deficits by targeting histone methyltransferases EHMT1/2 in Shank3-deficient mice. Mol. Psychiatry, https://doi.org/10.1038/s41380-019-0351-2, Epub ahead of print.

Wei, J., Xiong, Z., Lee, J.B., Cheng, J., Duffney, L.J., Matas, E., and Yan, Z. (2016). Histone modification of Nedd4 ubiquitin ligase controls the loss of AMPA receptors and cognitive impairment induced by repeated stress. J. Neurosci. *36*, 2119–2130.

Wess, J., Nakajima, K., and Jain, S. (2013). Novel designer receptors to probe GPCR signaling and physiology. Trends Pharmacol. Sci. *34*, 385–392.

Wesseling, H., Guest, P.C., Lee, C.M., Wong, E.H., Rahmoune, H., and Bahn, S. (2014). Integrative proteomic analysis of the NMDA NR1 knockdown mouse model reveals effects on central and peripheral pathways associated with schizophrenia and autism spectrum disorders. Mol. Autism *5*, 38.

Yizhar, O., Fenno, L.E., Prigge, M., Schneider, F., Davidson, T.J., O'Shea, D.J., Sohal, V.S., Goshen, I., Finkelstein, J., Paz, J.T., et al. (2011). Neocortical excitation/inhibition balance in information processing and social dysfunction. Nature *477*, 171–178.

Yuen, E.Y., Liu, W., Karatsoreos, I.N., Ren, Y., Feng, J., McEwen, B.S., and Yan, Z. (2011). Mechanisms for acute stress-induced enhancement of glutamatergic transmission and working memory. Mol. Psychiatry *16*, 156–170.

Yuen, E.Y., Wei, J., Liu, W., Zhong, P., Li, X., and Yan, Z. (2012). Repeated stress causes cognitive impairment by suppressing glutamate receptor expression and function in prefrontal cortex. Neuron *73*, 962–977.

Ziemba, B.P., Burke, J.E., Masson, G., Williams, R.L., and Falke, J.J. (2016). Regulation of PI3K by PKC and MARCKS: single-molecule analysis of a reconstituted signaling pathway. Biophys. J. *110*, 1811–1825.

Zou, H., Zhang, C., Xie, Q., Zhang, M., Shi, J., Jin, M., and Yu, L. (2008). Low dose MK-801 reduces social investigation in mice. Pharmacol. Biochem. Behav. *90*, 753–757.

Zhong, P., and Yan, Z. (2016). Distinct physiological effects of dopamine D4 receptors on prefrontal cortical pyramidal neurons and fast-spiking interneurons. Cereb. Cortex *21*, 62–70.

ISCI, Volume *17*

Supplemental Information

Chemogenetic Activation of Prefrontal Cortex in *Shank3*-Deficient Mice Ameliorates Social Deficits, NMDAR Hypofunction, and Sgk2 Downregulation

Luye Qin, Kaijie Ma, and Zhen Yan

Transparent Methods

All the details about experimental procedures are included in Supplemental Information.
Mice expressing C-terminal (exon 21) deleted Shank3 (Jackson Labs, Bar Harbor, ME) were maintained as previously described (Duffney et al., 2015; Qin et al., 2018; Wang et al., 2019). Since only the hemizygous deletion or loss-of-function mutation in the *Shank3* gene has been linked to human autism and intellectual disability (Durand et al., 2007), heterozygous Shank3$^{+/\Delta C}$ mice (6-8 weeks old, male) and age-matched wild-type male mice (C57BL/6, male) were used in this study. Mice of different genotypes were randomly assigned to CNO/saline groups. Experiments were carried out by investigators in a blind fashion (with no prior knowledge about the genotypes and treatments). All experiments were performed with the approval of the Institutional Animal Care and Use Committee (IACUC) of the State University of New York at Buffalo.

Behavioral Testing

Social Preference Test: A three-chamber social interaction assay was performed to assess social deficits (Duffney et al., 2015; Qin et al., 2018). Briefly, an apparatus (L: 101.6 cm, W: 50.8 cm, H: 50.8 cm) containing three chambers with retractable doorways allowing for access to side chambers was used. The test was composed of two phases with different stimulus in each of two side chambers. Each stimulus was placed inside a capsule (an inverted pencil cup, D: 10.2 cm, H: 10.5 cm). An upright plastic drinking cup was weighed down and placed on top of each capsule to prevent the subject mouse from climbing on top. The 1st phase contained two identical nonsocial stimuli (black folded papers), the 2nd phase contained a nonsocial (NS) stimulus (a wood block) and a social (Soc) stimulus (an age- and sex-matched wild-type mouse of the same strain). Locations of the NS and Soc stimuli were counterbalanced. Animals were habituated in the apparatus for two days before testing. During the habituation, two empty capsules were placed at side chambers, and animals were allowed to explore the central chamber for 10 minutes followed by an additional 10-min exploration with free access to all 3 chambers of the apparatus. During the sociability measurement, different stimuli were placed inside capsules at side chambers, and the test animal was placed in the center chamber, and was free to explore the apparatus for 10 minutes in each phase, while it was returned to home cage during the 5-min intervals between test phases. The chamber was cleaned with 75% Ethanol after each phase. Interaction time was counted based on “investigating” behaviors of the test animal to each stimulus. A computer running the Any-maze behavior tracking software (Stoelting, Wood Dale, IL) measured the time of the test animal spent at the close proximity of

the capsule (distance of animal head to cup edge: ≤3.5 cm). Preference index scores were calculated, where time spent with one stimulus was subtracted from the time spent with the other stimulus and divided by the total time spent exploring both stimuli.

Social Approach Test: The test animal was habituated in an apparatus (L: 67.7 cm, W: 50.8 cm, H: 50.8 cm) containing a capsule (an inverted pencil cup, placed in the center area) for 10 min, then was returned to the home cage. The apparatus was cleaned and a social stimulus (an age- and sex-matched wild-type mouse of the same strain) was placed inside the capsule. The test animal was put back into the apparatus to explore for 10 min. The time spent on interacting with the social stimulus was measured.

Rotarod Test: To assess motor coordination and balance, an accelerating rotarod (SD instruments, San Diego, CA) was used. Mice were placed on a cylinder, which slowly accelerated from 4 to 40 revolutions per minute over a 5-min test session. The task requires mice to walk forward in order to remain on top of the rotating cylinder rod.

Locomotion Test: The test animal was placed in the middle area of an apparatus (L: 67.7 cm, W: 50.8 cm, H: 50.8 cm) and freely exploring for 10 minutes, the total distance traveled were measured by Any-maze behavior tracking software (Stoelting, Wood Dale, IL).

Open Field Test: Animals were placed in the middle area of an apparatus (L: 67.7 cm, W: 50.8 cm, H: 50.8 cm) and freely exploring for 10 minutes, the amount of time the animal spent in the center (33.8 cm x 25.4 cm) was counted by Any-maze behavior tracking software (Stoelting, Wood Dale, IL). Anxious animals spend less time in the center and more time in the corner of the field.

Viral Vectors and Animal Surgery

The rAAV8-CaMKIIα-HA-hM3D(Gq)-mCherry and rAAV8-CaMKIIα-HA-hM4D(Gi)-mCherry were obtained from Addgene. The virus (1 μl) was bilaterally injected to the medial PFC (prelimbic and infralimbic regions) to infect glutamatergic neurons, as we described before (Wei et al, 2016; Wang et al., 2018). In brief, mice were anesthetized and placed on a stereotaxic apparatus (David Kopf Instruments, Tujunga, CA). The injection was carried out with a Hamilton syringe (needle gauge 31) at a speed of ~0.1 μl/min and the needle was kept in place for an additional 5min. The virus was delivered bilaterally to the PFC using the following coordinates: 1.9 mm anterior to the bregma, 0.25 mm lateral and 2.0 mm deep. Animals were allowed to recover for 2 days and used for experiments 2 weeks later. Clozapine N-oxide (CNO) or saline injection (i.p.) was given 1 hr before the start of behavioral testing or animal sacrifice for

electrophysiological recordings. Electrophysiological recordings were performed at 1-6 hours after intraperitoneal injection of CNO or saline in viral-infected mice.

Electrophysiological Recordings

Whole-cell voltage-clamp recording technique was used to measure synaptic currents in layer 5 pyramidal neurons of prefrontal cortical slices, as previously described (Yuen et al., 2012; Duffney et al., 2015; Qin et al., 2018). Mouse slices (300 μm) were positioned in a perfusion chamber attached to the fixed stage of an upright microscope (Olympus) and submerged in continuously flowing oxygenated ACSF (in mM: 130 NaCl, 26 $NaHCO_3$, 1 $CaCl_2$, 5 MgCl2, 3 KCl, 1.25 NaH_2PO_4, 10 glucose, pH 7.4, 300 mOsm). Bicuculline (20 μM) and CNQX (20 μM) were added in NMDAR-EPSC recordings. Patch electrodes contained internal solution (in mM): 130 Cs-methanesulfonate, 10 CsCl, 4 NaCl, 10 HEPES, 1 $MgCl_2$, 5 EGTA, 2 QX-314, 12 phosphocreatine, 5 MgATP, 0.2 Na_3GTP, 0.1 leupeptin, pH 7.2-7.3, 265-270 mOsm. Layer V mPFC pyramidal neurons were visualized with a 40X water-immersion lens and recorded with the Multiclamp 700A amplifier (Molecular Devices, Sunnyvale, CA). Evoked EPSC was generated with a pulse from a stimulation isolation unit controlled by a S48 pulse generator (Grass Technologies, West Warwick, RI). A bipolar stimulating electrode (FHC, Bowdoinham, ME) was placed ~100 μm from the neuron under recording. For NMDAR-EPSC, the cell (clamped at -70 mV) was depolarized to +40 mV for 3 s before stimulation to fully relieve the voltage dependent Mg^{2+} block. For input-output responses, EPSC was elicited by a series of pulses with different stimulation intensities (50-90 μA) delivered at 0.05 Hz. To record the spontaneous action potential (sAP), slices were bathed in a modified ACSF (in mM: 130 NaCl, 26 $NaHCO_3$, 1 $CaCl_2$, 0.5 $MgCl_2$, 3.5 KCl, 10 glucose, 1.25 NaH_2PO_4) to slightly elevate basal neuronal activity (Wei et al., 2018), which more closely mimics the ionic composition of brain interstitial fluid in situ (1.0-1.2 mM Ca^{2+},1 mM Mg^{2+}, and 3.5 mM K^+). Whole-cell current-clamp techniques were used to measure action potential firing with the internal solution containing (in mM: 20 KCl, 100 K-gluconate, 10 HEPES, 4 ATP, 0.5 GTP, and 10 phosphocreatine (Zhong and Yan, 2016). A small depolarizing current was applied to adjust the interspike potential to -60 mV. Data analyses were performed with Clampfit (Axon instruments, Molecular Devices, Sunnyvale, CA) and GraphPad Prism 6 (GraphPad Software, Inc., La Jolla, CA).

Quantitative Real-time RT-PCR

To compare the mRNA levels, quantitative RT-PCR was used. Total RNA was isolated from mouse PFC punches using Trizol reagent (Invitrogen) and treated with DNase I (Invitrogen) to

remove genomic DNA. Then iScript™ cDNA synthesis Kit (Bio-Rad) was used to obtain cDNA from the tissue mRNA. Quantitative real time PCR was carried out using the iCycler iQ™ Real-Time PCR Detection System and iQ™ Supermix (Bio-Rad) according to the manufacturer's instructions. In brief, *GAPDH* was used as the housekeeping gene for quantitation of the expression of target genes in samples from WT vs. Shank3$^{+/\Delta C}$ mice treated with CNO or saline. Fold changes in the target genes were determined by: Fold change = $2^{-\Delta(\Delta C\ T)}$, where $\Delta CT = CT_{(target)} - CT_{(GAPDH)}$, and $\Delta(\Delta CT) = \Delta CT_{(treated)} - \Delta CT_{(WT+saline)}$. CT (threshold cycle) is defined as the fractional cycle number at which the fluorescence reaches 10x the standard deviation of the baseline. A total reaction mixture of 20 μl was amplified in a 96-well thin-wall PCR plate (Bio-Rad) using the following PCR cycling parameters: 95°C for 5 min followed by 40 cycles of 95°C for 45 sec, 55°C for 45 sec, and 72°C for 45 sec. Primers for GAPDH are as follows: 5-GACAACTCACTCAAGATTGTCAG-3 (forward); 5-ATGGCATGGACTGTGGTCATGAG-3 (reverse). Primers for Sgk1 are as follows: 5-CTGTTGAAGAATGTGAAGCA-3 (forward); 5-CCTCTGGAGATGGTAGAACA-3 (reverse); Primers for Sgk2 are as follows: 5-AACCACATGTTCTTCAGTCC-3 (forward); 5-CAAAGTGTTTCAAGTCAGCA-3 (reverse). Primers for Sgk3 are as follows: 5-GAAGAGCAGGATTGAATGAG-3 (forward); 5-ATGTTCCGTGAGGTAGAATG -3 (reverse); Primers for CaMKIIα are as follows: 5-GAATCTTCTGAGAGCACCAA-3 (forward); 5-TGTAGGACTCAAAGTCTCCA-3 (reverse); Primers for Fyn are as follows: 5-ATATTGAACAGCTCGGAAGG-3 (forward); 5-GCCAAGTTTTCCAAAGTACC-3 (reverse); Primers for Homer1b are as follows: 5-AACACAAAGAAGAACTGGGT-3 (forward); 5-ATTGCCTTTGAGCCATCTAA-3 (reverse); Primers for Homer1a are as follows: 5-GGCAAACACTGTTTATGGAC-3 (forward); 5-GAGACTGAAGATCTCCTCCT-3 (reverse); Primers for Arc are as follows: 5-GAGGCTCAGCAATATCAGTC-3 (forward); 5-GGACAGCCAATATTCTTCAG-3 (reverse).

Immunohistochemistry

Mice were anesthetized and transcardially perfused with PBS, followed by 4% paraformaldehyde (PFA) prior to brain removal. Brains were post-fixed in 4% PFA for 2 days and cut into 100 μm slices. Slices were cut coronally, washed and blocked for 1 hour in PBS containing 3% BSA. After washing, slices were incubated with the primary antibody against NR2A (1:500, Millipore, 07-632) or GluR2 (1:500, AB1506), PSD-95 (1:500, Cell signaling, 36233) for 72 hours at 4°C. After washing 3 times in PBS, slices were incubated with secondary antibodies (Alex488, 1:1000, Invitrogen, A11008; Alex594, 1:1000, Invitrogen, A11032) for 2 hours at room temperature, followed by 3 washes with PBS. Slices were mounted on slides with

VECTASHIELD mounting media containing DAPI (Vector Laboratories). Images were acquired using a 40X objective on a Zeiss LSM 510 Confocal Microscope. All specimens were imaged under identical conditions and analyzed with identical parameters using Image J software. Z-axis stacked confocal images from 1-2 slices per animal were quantified.

Statistics

All data were expressed as the mean ± SEM. No sample was excluded from the analysis. The sample size was based on power analyses and was similar to those reported in previous works (Duffney et al., 2015; Wei et al., 2016; Yuen et al., 2012; Qin et al., 2018). The variance between groups being statistically compared was similar. Experiments with two groups were analyzed statistically using unpaired Student's *t*-tests. Experiments with more than two groups were subjected to one-way ANOVA, two-way ANOVA, or two-way repeated measure ANOVA (rmANOVA), followed by *post hoc* Bonferroni tests.

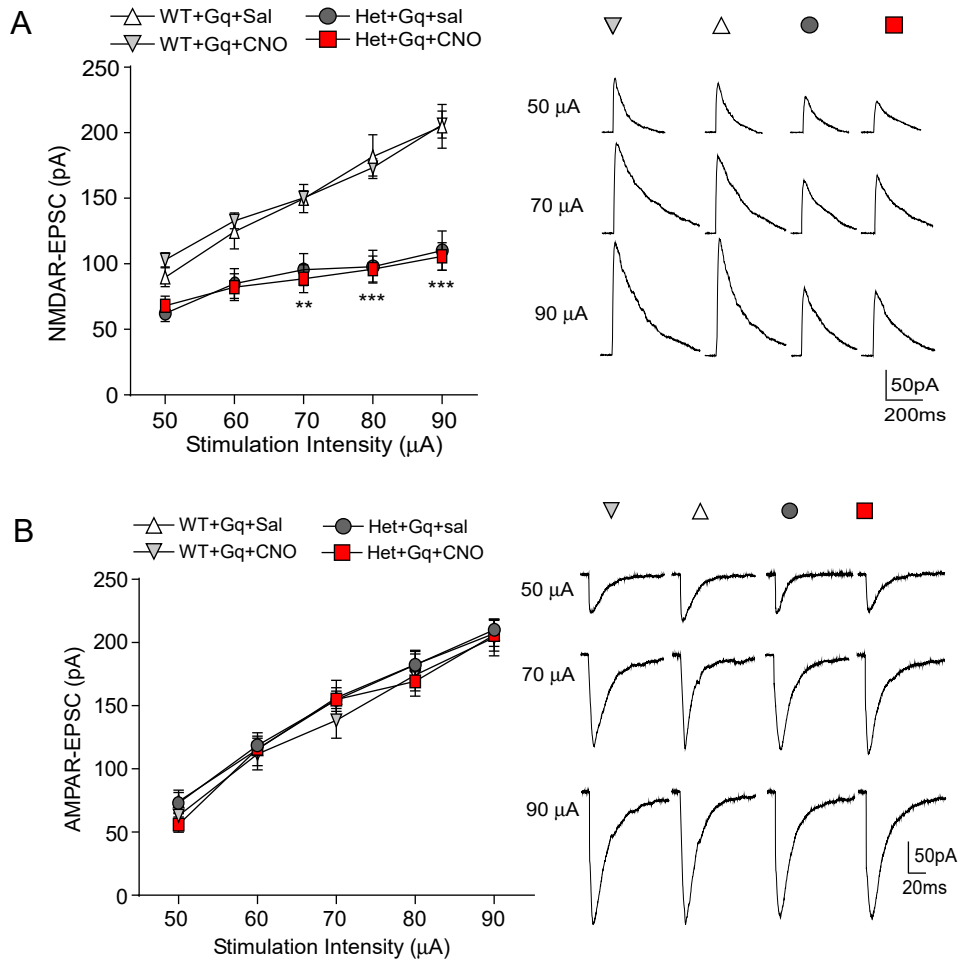

Figure S1. Effect of chemogenetic activation of PFC pyramidal neurons on NMDAR and AMPAR function at a late time point, related to Figure 2 and Figure 3. (A, B) Summarized input-output curves of NMDAR-EPSC (A) or AMPAR-EPSC (B) in layer V PFC pyramidal neurons from WT vs. Shank3-deficient mice (Het, hM3Dq-injected) treated with saline or CNO for 24 hours. **p<0.01, ***p<0.001, two-way rmANOVA.

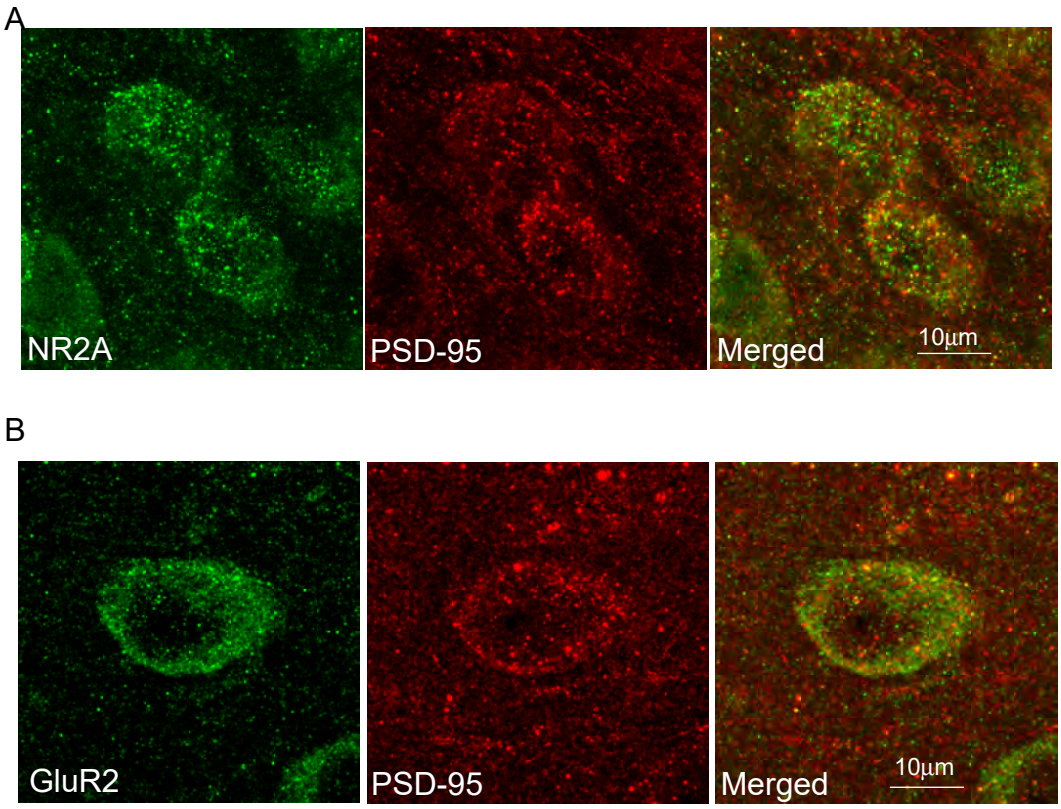

Figure S2. Co-localization of NR2A or GluR2 with a synaptic marker, related to Figure 2 and Figure 3. (A, B) Representative confocal images of NR2A (A) or GluR2 (B) co-staining with PSD-95 in PFC slices of WT mice.

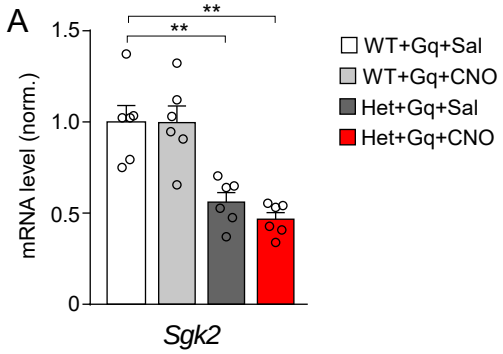

Figure S3. Effect of chemogenetic activation of PFC pyramidal neurons on *Sgk2* expression at a late time point, related to Figure 4. (A) Quantitative PCR showing mRNA level of *Sgk2* in WT vs. Shank3-deficient mice (Het, hM3Dq-injected) treated with saline or CNO (3 mg/kg, i.p.) for 24 hours. **p<0.01, two-way ANOVA.